Analysis of the Seeded Combustion Gas Boundary Layer Near a Cold Electrode

Ken Okazaki,* Yasuo Mori,† Kazutomo Ohtake,‡ and Kunio Hijikata§
Tokyo Institute of Technology, Tokyo, Japan

The boundary layer of potassium-seeded combustion gas over a cold electrode under the condition of diffusive current mode without arcs is studied theoretically and experimentally. The theoretical analysis features the introduction of charge separation between electrons and ions, electron thermal nonequilibrium, finite ionization rate, and no assumption of thin sheath layer adjoining the electrode surface. To simplify the problem, the case when the current is produced by an applied external electric field without a magnetic field is studied. In this paper, because of the reliability and suitability of the electric boundary condition adopted in the analysis, the boundary layer around the anode is specifically taken up. For the laminar boundary layer, numerical results for the colder electrode and smaller seed fraction show that the region of the electron-ion charge separation extends much wider than the Debye length from the surface and that both electron thermal and ionizational nonequilibria are considerably remarkable near the electrode even in the seeded combustion gas, and the calculated performance of the electrode voltage drop and current density agrees fairly well with experimental results. On the other hand, for the turbulent boundary layer under the condition of practical MHD generator operation, it is shown from numerical calculations that the charge separation region is limited to the extent of several Debye lengths from the surface and that the electron number density is very close to that obtained by Saha equation for the electron temperature.

Nomenclature

C_p = specific heat at constant pressure
D = diffusion coefficient in the gas
E = electric field vector (the component in y direction is E)
J = total current density vector (the component in y direction is J)
k = Boltzmann's constant
M = molecular weight of the gas
m = particle mass
N_0 = Avogadro number
n = particle number density
P = pressure
Q_{ex} = collision cross section for momentum exchange between electron and species X
R = universal gas constant
Re_x = Reynolds number
T = temperature
u = mass average velocity vector [$u = (u,v)$]
X_K = mole fraction of potassium atom
α = recombination coefficient
Γ = particle flux vector
δ = turbulent boundary-layer thickness
δ_x = electron energy-loss factor of species X
ϵ = permittivity of free space
ϵ_i = ionization energy
λ = thermal conductivity
μ = viscosity
μ_e, μ_i = mobilities of electron and ion
$\bar{\nu}_{ex}$ = averaged collision frequency between electron and species X
ρ = mass density

Subscripts

e = electron
i = ion
x = species X
s = Saha equilibrium
∞ = main flow condition
w = wall or surface condition

Received April 25, 1977; revision received Aug. 22, 1977.
Index categories: MHD; Plasma Dynamics and MHD.
*Graduate Student, Dept. of Physical Engineering.
†Professor, Dept. of Physical Engineering.
‡Assistant Professor, Dept. of Physical Engineering.
§Associate Researcher, Dept. of Physical Engineering.

I. Introduction

IN the research and development of MHD power generation, one of the most important problems is the duration of the electrode, and cold or semihot electrodes have been attracting attention. Therefore, it is very important to investigate the boundary layer of seeded combustion gas over the cold or semihot electrode. MHD boundary layers of gas plasma have been analyzed in some detail under the condition of electron thermal nonequilibrium and finite ionization rate. Sherman et al.[1] analyzed a steady two-dimensional laminar boundary layer of cesium-seeded argon plasma without assuming local similarity. But, in their electron continuity equation the diffusion term was neglected, and so the wall boundary condition for it was not necessary. Brown,[2] Cotte,[3] and High et al.[4] took ambipolar diffusion into consideration in the electron continuity equation on a boundary condition that required the electron flux to be matched to that across the sheath. These analyses have been developed on the assumption that the sheath thickness is of the same order of magnitude with or less than the Debye length. In the case when the current density is high enough in the boundary layer on a cold electrode, the strong electric field is set up in the low electrical conductivity zone near the surface, which is considered to bring about a large electron-ion charge separation, an extension of charge separation region much wider than expected, and an elevation of the electron temperature above the heavy particle temperature even in the seeded combustion gas containing many polyatomic molecules. The electron temperature nonequilibrium was also pointed out by Argyropoulos et al.[5] who reported a significant electron temperature elevation above the gas temperature in the high-current region in the open-cycle MHD generator. In addition to these facts, it should be pointed out that because of the low electron number density in the colder zone of the boundary layer, ionization and recombination rates would be too small

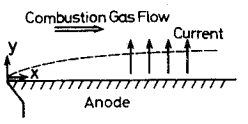

Fig. 1 Coordinate system.

to maintain the equilibrium concentration of electrons or ions at the local electron temperature.

The main purpose of this study is to analyze the boundary layer with least assumptions in consideration of the phenomena mentioned, such as electron-ion charge separation, electron thermal and ionization nonequilibria, and electron-heavy particle collisional ionization in the seeded combustion gas boundary layer over a cold electrode. Under the condition of diffusive current mode, the analysis is mainly focused on the two-dimensional laminar boundary layer with an applied electric field to emphasize the factors described. The calculated relation of voltage-current is compared with experimental results made in the laminar region. Finally, an analysis of turbulent boundary layer is made under the condition of practical open-cycle MHD generator operation and the results are discussed.

II. Theoretical Analysis

A. Basic Equations

The steady two-dimensional laminar boundary layer over a flat-plate cooled anode is assumed as shown in Fig. 1. In the main flow the velocity, the gas temperature, and the pressure are constant along the flow direction; and the electric field is applied between the main flow and the anode. The gas consists of electrons, single ionized ions of seed, and neutral heavy polyatomic molecules. In the analysis no assumption is made about charge neutrality or sheath, but the ion and electron conservation equations are introduced. Concerning the electron energy equation, because of the low electron density and the fairly large electric field in the cold zone of the boundary layer near the electrode and of the extremely large electron energy-loss factor of the electron-heavy particle collision, a dominant mechanism in the electron energy exchange is the local energy balance between the energy gained from the electric field and the energy loss by inelastic collisions with heavy particles. The electron thermal conductivity is approximately in proportion to the electron number density and the electron thermal velocity, and in the calculation of the cold boundary layer under the condition similar to that of the MHD generator, the electron number density is 10^{16}-10^{20} m^{-3}, and the electron temperature is 1000-3000 K. Therefore, the term of the electron thermal conduction is found to be below 1% of the Joule heating term through the whole boundary layer, including the range of large electron temperature gradient near the surface. Under this condition, the radiation loss in the electron energy balance is about 1% of the Joule heating for 10 A/m^2 at most. The effects by convection and diffusion processes are much smaller than that of the radiation loss. The contribution of electrons or ions to the overall energy equation is considered to be caused only by the Joule heating. The viscous dissipation term in the overall energy equation is neglected.

Based on the conditions just described, the basic equations are written as follows:

Overall continuity equation

$$\frac{\partial(\rho u)}{\partial x}+\frac{\partial(\rho v)}{\partial y}=0 \tag{1}$$

Overall momentum equation

$$\rho u\frac{\partial u}{\partial x}+\rho v\frac{\partial u}{\partial y}=\frac{\partial}{\partial y}\left(\mu\frac{\partial u}{\partial y}\right) \tag{2}$$

Overall energy equation

$$\rho uC_p\frac{\partial T}{\partial x}+\rho vC_p\frac{\partial T}{\partial y}=\frac{\partial}{\partial y}\left(\lambda\frac{\partial T}{\partial y}\right)+\boldsymbol{J}\cdot\boldsymbol{E} \tag{3}$$

Equation of state

$$P=\rho(R/M)T \tag{4}$$

Electron continuity equation

$$\nabla\cdot(n_e\boldsymbol{u}_e)=\dot{n}_e \tag{5}$$

Ion continuity equation

$$\nabla\cdot(n_i\boldsymbol{u}_i)=\dot{n}_i \tag{6}$$

Poisson's equation

$$\nabla\cdot\boldsymbol{E}=(e/\epsilon)(n_i-n_e) \tag{7}$$

Electron energy equation

$$\boldsymbol{J}\cdot\boldsymbol{E}=\sum_x\delta_x\bar{\nu}_{ex}n_e\frac{3}{2}k(T_e-T) \tag{8}$$

The left sides of Eqs. (5) and (6) are expressed by the sum of the fluxes of convection, drift, and diffusion as follows:

$$n_e\boldsymbol{u}_e=n_e\boldsymbol{u}-n_e\mu_e\boldsymbol{E}-\rho D_e\nabla\left(\frac{N_e}{\rho}\right) \tag{9}$$

$$n_i\boldsymbol{u}_i=n_i\boldsymbol{u}+n_i\mu_i\boldsymbol{E}-\rho D_i\nabla\left(\frac{n_i}{\rho}\right) \tag{10}$$

The production terms in the right sides of Eqs. (5) and (6) are expressed by n_e, T_e, T, and concentration of heavy particles, and will be discussed later. Therefore, when the value for $\boldsymbol{J}$ is given, Eqs. (1-8) and $\nabla\times\boldsymbol{E}=0$ constitute a closed set of coupled equations for the eight unknown quantities of $\rho,u,v,T,n_e,n_i,\boldsymbol{E}$, and T_e. In the calculation, the gas dynamical quantities such as ρ,u,v, and T are determined from Eqs. (1-4) considering $\boldsymbol{J}\cdot\boldsymbol{E}$ as an iterated term, and then $n_e,n_i,\boldsymbol{E}$, and T_e are obtained from Eqs. (5-8). However, since it is not easy to solve Eqs. (5-8), these equations are so rearranged as to be more easily solved by a computer.

Dividing Eq. (9) by μ_e and Eq. (10) by μ_i, adding these equations, and considering the inequality $\mu_e\gg\mu_i$, we obtain

$$n_e\boldsymbol{u}_e+(\boldsymbol{J}/e)=n_e\boldsymbol{u}+(n_i-n_e)\boldsymbol{u}+\mu_i(n_i-n_e)\boldsymbol{E}$$
$$-\left[\frac{\rho\mu_ikT}{e}\left(1+\frac{T_e}{T}\right)\nabla\left(\frac{n_e}{\rho}\right)+\frac{\rho\mu_ikT}{e}\nabla\left(\frac{n_i-n_e}{\rho}\right)\right] \tag{11}$$

In the process of the introduction of Eq. (11), the following Einstein relations are used:

$$\frac{D_i}{\mu_i}=\frac{kT}{e},\quad\frac{D_e}{\mu_e}=\frac{kT_e}{e}$$

Noting that n_i-n_e does not vanish but is given by Eq. (7), we obtain the following electron continuity equation:

$$\rho\boldsymbol{u}\cdot\nabla Y_e+\frac{m_e\epsilon}{e}\nabla\cdot\{(\nabla\cdot\boldsymbol{E})\boldsymbol{u}\}+\nabla\cdot\left[\frac{\epsilon\mu_im_e}{e}(\nabla\cdot\boldsymbol{E})\boldsymbol{E}\right.$$
$$\left.-\frac{\mu}{Sc_i}\left(1+\frac{T_e}{T}\right)\nabla Y_e-\frac{\mu}{Sc_i}\frac{\epsilon m_e}{e}\nabla\left(\frac{\nabla\cdot\boldsymbol{E}}{\rho}\right)\right]=m_e\dot{n}_e \tag{12}$$

where Y_e and Sc_i are the electron mass fraction and ion Schmidt number, respectively. In the left-hand side of Eq. (12) the second term is much smaller than the third term and is neglected, because the inequality $\nabla \cdot \boldsymbol{u} \ll \nabla \cdot (\mu_i \boldsymbol{E})$ holds in the region close to the surface where the charge separation is significant and $\nabla \cdot \boldsymbol{E}$ gets smaller in the outer layer. The terms including $\nabla \cdot \boldsymbol{E}$ have been neglected in the analyses reported so far, but especially the first term in the bracket is found to be very important for some conditions near the surface according to the numerical results described later and is not omitted in our analysis.

Subtracting Eq. (5) from Eq. (6) by use of the relation $\dot{n}_e = \dot{n}_i$, we obtain $\nabla \cdot \boldsymbol{J} = 0$, where $\boldsymbol{J}$ is the total current density vector and is expressed as

$$\boldsymbol{J} = e(n_i - n_e)\boldsymbol{u} + en_i\mu_i\boldsymbol{E} + en_e\mu_e\boldsymbol{E} - e\rho D_i \nabla (n_i/\rho) + e\rho D_e \nabla (n_e/\rho) \tag{13}$$

The fluxes of ion diffusion and ion drift in Eq. (13) are much smaller than that of electron drift, and from investigation of the order of magnitude of the electron diffusion term, it is made sure that the electron diffusion flux is one order of magnitude smaller than the drift flux for $J = 10\ \mathrm{A/m^2}$ and the contribution of the electron diffusion flux gets much smaller for higher current densities. Besides, in the region close to the surface where significant charge separation is expected to occur and the gas velocity is much smaller than the electron drift velocity, the third term is the only dominant term in the right-hand side of Eq. (13). So we obtain

$$\boldsymbol{J} = e\, n_e \mu_e \boldsymbol{E} \tag{14}$$

Finally, Eqs. (12) and (14) constitute the basic equations for the unknown quantities n_e and $\boldsymbol{E}$. Once n_e and $\boldsymbol{E}$ are obtained from these equations, then n_i can be calculated by Eq. (7).

For the seeded combustion gas, Pr and Sc_i are assumed constant at 0.73 and 1.5, respectively. The data for the electron energy-loss factor δ_x are quoted from a paper by Maxwell et al.[6] The potassium ion mobility is obtained on referring to McDaniel et al.[7] On calculating the electron mobility, the electron-heavy particle momentum transfer cross sections are quoted from the table arranged by Spencer et al.[8]

In the problem we are dealing with, the following other two important points should be discussed before carrying out numerical computation. One is the boundary condition at the electrode surface, and the other is the ionization rate. These two items are investigated in detail.

B. Boundary Conditions

In the main flow the electron density is large enough so that the electron thermal and ionization equilibria are attained, then the boundary conditions on the outer edge of the boundary layer are specified as follows:

$$y \to \infty:\ u = u_\infty,\ T = T_\infty,\ n_e = n_{es}(T_\infty),\ \nabla\left(\frac{n_i - n_e}{\rho}\right) = 0$$

where u_∞ and T_∞ are constant along the x direction and the suffix s means the value given by Saha equation. The boundary condition at the surface for the electron continuity equation should be carefully derived. When the current density is as small as in the analysis of probe performance, the condition of $n_i = 0$ might be assumed.[9] However, for the higher current density, since ions do not enter into and go out of the electrode, the net ion flux at the anode surface must vanish, but n_e and n_i are not necessarily required to be zero. Then, as the boundary conditions at the surface we have

$$y = 0:\ u = v = 0,\ T = T_w,\ \Gamma_{iw} = 0$$

The boundary conditions of $\Gamma_{iw} = 0$ at the surface are rearranged by use of Eqs. (9) and (10) by means similar to the derivation of Eq. (12), and the following equation is obtained to be used as the boundary condition at the surface:

$$\frac{\epsilon\mu_i m_e}{e}(\nabla \cdot \boldsymbol{E})\boldsymbol{E} - \frac{\mu}{Sc_i}\left(1 + \frac{T_e}{T}\right)\nabla Y_e - \frac{\mu}{Sc_i}\frac{\epsilon m_e}{e}\nabla\left(\frac{\nabla \cdot \boldsymbol{E}}{\rho}\right) = -\frac{m_e\mu_i}{e\mu_e}\boldsymbol{J}$$

As for the surface temperature, the two cases should be considered making reference to the cooled electrode of MHD power generators. One is the case when the electrode surface directly contacts with the gas and T_w is kept at 700 K by cooling. The other is the case when the electrode surface is covered with the thin layer of condensed seed material such as K_2CO_3 and the surface temperature T_w is given by the saturation condition of the vapor pressure of seed material and is about 1200 K for K_2CO_3 in the MHD generator.

C. Ionization Rate

In connection with $\dot{n}_e$, the three-body recombination when the third body is an electron has been considered so far to be the dominant reaction in general under the condition of open-cycle MHD power generation, but the contribution of the reaction when the third body is a heavy particle X has not been seriously discussed. However, in the cold region near the surface where the electron number density is small and the former reaction rate is small, the latter reaction could be significant. When both reactions are taken into account, the electron or ion production rate per unit volume is written as follows:

$$\dot{n}_e = (\alpha_e + \alpha_x)(n_{es}^2 - n_e n_i) \tag{15}$$

where n_{es} is the electron number density in the Saha equilibrium at the electron temperature. The recombination coefficient α_e corresponds to the case when the third body is an electron and is given by Hinnov et al.[10] as

$$\alpha_e = 1.09 \times 10^{-20} n_e T_e^{-9/2}\ [\mathrm{m^3/s}] \tag{16}$$

where n_e is in $\mathrm{m^{-3}}$ and T_e is in K. The recombination coefficient α_x is that for a heavy particle X for which there is insufficient data; therefore, its value is calculated based on the theory by Thomson.[11] The total relative energy equation of the electron and the ion at the distance r is given by $E_0 = E_k - e^2/4\pi\epsilon r$, where $E_0 = 3/2\ kT_e$ is the total relative energy at infinity, and E_k is the relative kinetic energy at distance r. When $3/2\ kT$ is the kinetic energy of the third body X and δ_x is the electron inelastic energy loss factor, the critical radius r_0 for the collision of electron and particle X is obtained from the equation $\delta_x(E_k - 3/2kT) \geq 3/2kT_e$ as

$$r_0 = \left(\delta_x \cdot \frac{e^2}{4\pi\epsilon}\right) \Big/ \left[\frac{3}{2}kT_e - \delta_x \cdot \frac{3}{2}k(T_e - T)\right] \tag{17}$$

where the second term of the denominator is smaller enough compared with the first term and is approximately neglected within the accuracy of several percentage points, because δ_x is 0.1 at most for any molecule of the combustion gas and $T_e > T_e - T$. Taking into account the probability that the electron will make a thermalizing collision with the X particle within the distance r_0 from the ion, we obtain the expression for α_x as

$$\alpha_x = \frac{16}{9}\sqrt{\frac{8\pi k}{m_e}}\left[\frac{2}{3k} \cdot \frac{e^2}{4\pi\epsilon}\right]^3 \frac{N_0}{R}\left[\sum_x \delta_x{}^3 X_x Q_{ex}\right] PT^{-1} T_e^{-5/2} \tag{18}$$

In this expression, the main contribution of $\delta_x{}^3$ is by CO_2 molecules in the combustion gas. This type of recombination process is significant only in the cold region.

D. Nondimensional Equations

To solve the basic equations numerically, the equations are made nondimensional. To use the Howarth transformation, we introduce

$$\xi = \int_0^x (\rho\mu)_\infty u_\infty \mathrm{d}x \tag{19}$$

$$\eta = \frac{u_\infty}{\sqrt{2\xi}} \int_0^y \rho \mathrm{d}y \tag{20}$$

The following nondimensional forms for the dependent variables are also introduced:

$$f' = \frac{u}{u_\infty}, \quad f = \int_0^\eta f' \mathrm{d}\eta, \quad \theta = \frac{T - T_w}{T_\infty - T_w}$$

$$\theta = \frac{T}{T_\infty}, \quad \theta_e = \frac{T_e}{T_\infty}, \quad \zeta = \frac{Y_e}{Y_{e\infty}}$$

Then the basic Eqs. (1-3, 8, and 12) are transformed into the following forms:

$$2\xi \frac{\partial f'}{\partial \xi} + \frac{\partial V}{\partial \eta} + f' = 0 \tag{21}$$

$$2\xi f' \frac{\partial f'}{\partial \xi} + V \frac{\partial f'}{\partial \eta} = \frac{\partial}{\partial \eta}\left(C_1 \frac{\partial f'}{\partial \eta}\right) \tag{22}$$

$$2\xi f' \frac{\partial \Theta}{\partial \xi} + V \frac{\partial \Theta}{\partial \eta} = \frac{\partial}{\partial \eta}\left(C_2 \frac{\partial \Theta}{\partial \eta}\right) + H \tag{23}$$

$$2\xi f' \frac{\partial \zeta}{\partial \xi} + V \frac{\partial \zeta}{\partial \eta} = \frac{\partial}{\partial \eta}\left[A_1 \frac{1}{\zeta^3} \frac{\partial \zeta}{\partial \eta} + A_2\left(1 + \frac{\theta_e}{\theta}\right) \frac{\partial \zeta}{\partial \eta}\right.$$

$$\left. + A_3 \frac{\partial}{\partial \eta}\left(\frac{1}{\zeta^2} \frac{\partial \zeta}{\partial \eta}\right)\right] + F \tag{24}$$

$$G \frac{1}{\zeta^2} = \frac{\sqrt{\theta_e}}{\theta^3}(\theta_e - \theta) \tag{25}$$

where

$$V = \frac{2\xi}{(\rho\mu)_\infty u_\infty}\left(f' \frac{\partial \eta}{\partial x} + \frac{\rho v}{\sqrt{2\xi}}\right)$$

$$C_1 = \frac{\rho\mu}{(\rho\mu)_\infty}$$

$$C_2 = \frac{\rho\mu}{(\rho\mu)_\infty} \frac{1}{Pr}$$

$$H = \frac{2\xi \boldsymbol{J} \cdot \boldsymbol{E}}{\rho u_\infty^2 (\rho\mu)_\infty C_p (T_\infty - T_w)}$$

$$A_1 = \frac{1}{(\rho\mu)_\infty} \frac{\epsilon \mu_i J^2}{e^3 \mu_e^2} \frac{\rho_\infty^3}{\rho n_{e\infty}{}^3}$$

$$A_2 = \frac{\rho\mu}{(\rho\mu)_\infty} \frac{1}{Sc_i}$$

$$A_3 = -\frac{\rho\mu}{(\rho\mu)_\infty} \frac{1}{Sc_i} \frac{\epsilon J}{e^2 \mu_e} \frac{u_\infty}{\sqrt{2\xi}} \frac{\rho_\infty^2}{\rho n_{e\infty}{}^2}$$

$$F = \frac{2\xi m_e \dot{n}_e}{\rho u_\infty^2 (\rho\mu)_\infty Y_{e\infty}}$$

$$G = \frac{J^2}{2e n_{e\infty}{}^2 \mu_e P \left(\frac{8kT_\infty}{\pi m_e}\right)^{1/2} \sum_x \delta_x X_x Q_{ex}}$$

Considering the relation of $n_e n_i = n_e^2 + (\epsilon/e) n_e \nabla \cdot \boldsymbol{E}$, the electron production rate given by Eq. (15) is transformed as

$$\dot{n}_e = (\alpha_{e\infty} \zeta \theta_e{}^{-9/2} + \alpha_{x\infty} \theta_e{}^{-5/2}) n_{e\infty}{}^2 \theta^{-3} (\zeta_s{}^2 - \zeta^2)$$

$$+ (\alpha_{e\infty} \zeta \theta_e{}^{-9/2} + \alpha_{x\infty} \theta_e{}^{-5/2}) \frac{\epsilon J}{e^2} \frac{\rho_\infty}{\mu_e} \frac{u_\infty}{\sqrt{2\xi}} \theta^{-2} \frac{1}{\zeta} \frac{\partial \zeta}{\partial \eta} \tag{26}$$

Local similarity and Howarth approximation of $\rho\mu = \text{const.}$ are assumed in the analysis because they are considered to hold a fairly good approximation in the study of a boundary layer when no magnetic field is applied and physical properties vary considerably through the layer.

The boundary conditions are also transformed as

$$\eta \to \infty : f' = 1, \ \Theta = 1, \ \zeta = 1, \ \frac{\partial}{\partial \eta}\left(\frac{1}{\zeta^2} \frac{\partial \zeta}{\partial \eta}\right) = 0$$

$$\eta = 0 : f = f' = 0, \ \Theta = 0, \ A_1 \frac{1}{\zeta^3} \frac{\partial \zeta}{\partial \eta} + A_2\left(1 + \frac{\theta_e}{\theta}\right) \frac{\partial \zeta}{\partial \eta}$$

$$+ A_3 \frac{\partial}{\partial \eta}\left(\frac{1}{\zeta^2} \frac{\partial \zeta}{\partial \eta}\right) = Z$$

where

$$Z = \frac{1}{(\rho\mu)_\infty} \frac{\sqrt{2\xi} \mu_i J}{e \mu_e u_\infty} \frac{\rho_\infty}{n_{e\infty}}$$

The electron energy equation [Eq. (25)] and electron continuity equation obtained from Eq. (24) are simultaneously integrated by the Runge-Kutta-Gill method from the outer edge of the boundary layer with an assumed initial value $(\partial\zeta/\partial\eta)_\infty$ so as to satisfy the inner boundary condition.

III. Experiment

A kerosene combustion gas, seeded with KOH and fired with oxygen-enriched air, was introduced into the measuring section consisting of a pair of flat-plate parallel-segmented electrodes as shown in Fig. 2. The temperature of the main flow was measured by the Na-D line reversal method and the

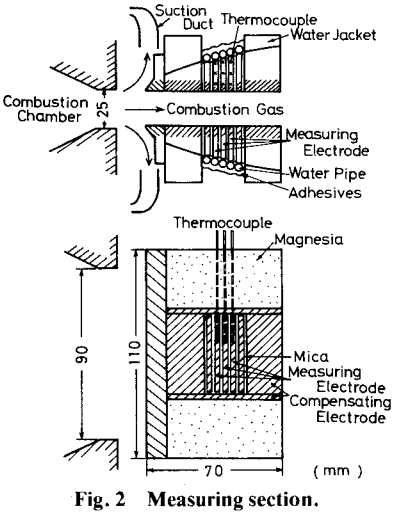

Fig. 2 Measuring section.

velocity was calculated from the temperature and the flow rate. The flow was confirmed to be laminar from measurements of temperature profile by Pt-Pt/Rh thermocouples. The electrode-block heights of segmented electrodes are so designed as to hold the wall temperature constant along the flow direction. Heat flux is calculated from the temperature gradient obtained from the readings of three thermocouples set in each of the three segmented stainless-steel electrodes. The mode of diffusive current or arc mode was recognized from the current fluctuation and the observation of the electrode surface. The wall temperature was calculated by the extrapolation of the temperature profile in the electrode.

Most of the experiments were carried out under conditions where the main flow velocity was 40 m/sec, the temperature 2300 K, the potassium atom mole fraction 0.03%, and the wall temperature 700 K. The reason why the mole fraction is small is that otherwise steady measurements could not be accomplished because of an unsteady thicker layer of condensed seed material on the electrode. From measurements by an electrical floating probe inserted in the main flow, the anode drop was found to be much smaller than the cathode drop especially at the low applied voltage as shown in Fig. 3.

The data obtained in this experiment was compared with theoretical results in the following section.

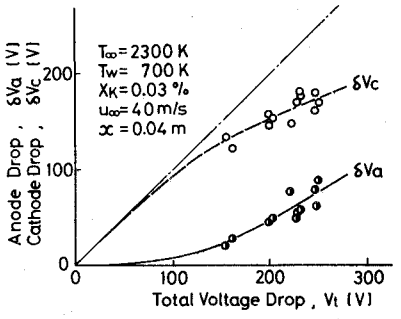

Fig. 3 Anode drop and cathode drop vs applied total voltage.

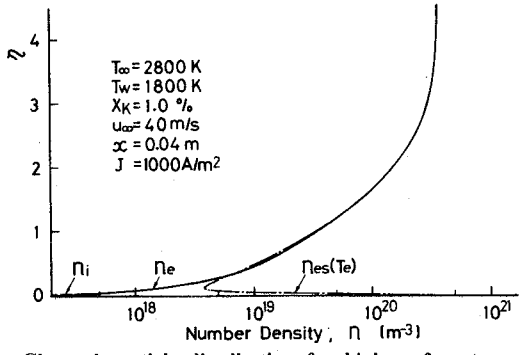

Fig. 4 Charged particle distribution for high surface temperature and large seed fraction.

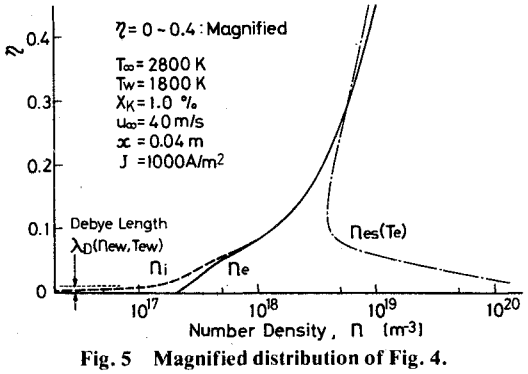

Fig. 5 Magnified distribution of Fig. 4.

IV. Numerical Results

A. Laminar Boundary-Layer Analysis

Numerical calculations were made on several characteristic conditions. The first case was done in order to show the prevalence of the charge neutrality throughout almost all of the region and the sheath thickness being of the same order of magnitude with the Debye length. The calculation was performed under condition of high electrode temperature and high seed fraction. The results for $T_\infty = 2800$ K, $T_w = 1800$ K, potassium atom mole fraction $X_K = 1.0\%$, and $J = 1000$ A/m^2 are shown in Figs. 4 and 5. (In Fig. 5, the ordinate is ten times as large as that of Fig. 4.) These results correspond to the conventional concepts in the combustion plasma showing that, except in the very thin sheath, the thickness of which is about of the same order with the Debye length, the electron thermal and ionization equilibria are attained with the electrical neutrality.

The second case was selected to make a comparison with the experimental result described earlier. The results of the electron and ion number densities on condition of $T_\infty = 2300$ K, $T_w = 1200$ K, and $X_K = 0.03\%$, which coincide with our experimental conditions are shown in Figs. 6-8 for $J = 20$

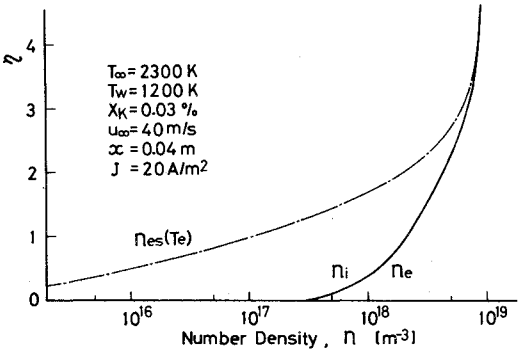

Fig. 6 Charged particle distribution for small current density.

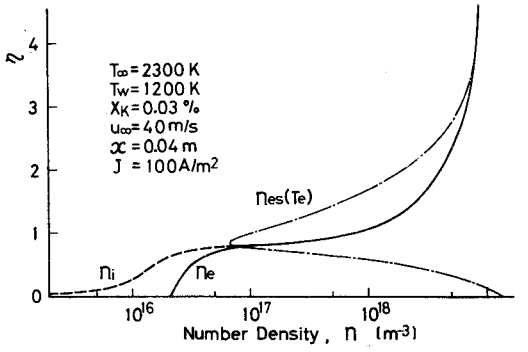

Fig. 7 Charged particle distribution for medium current density.

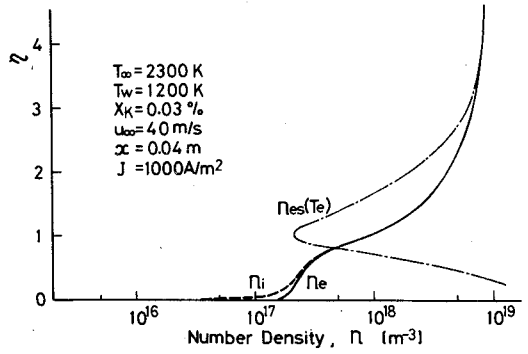

Fig. 8 Charged particle distribution for large current density.

A/m^2, 100 A/m^2, and 1000 A/m^2, where $n_{es}(T_e)$ is the Saha equilibrium electron number density for the local electron temperature. These results show that the charge separation region, which is negligibly thin for the very low current density, grows much larger than the Debye length with an increase in the current density. However, for the much higher current density, the charge separation region seems apparently to disappear, but in the separation region the value of the difference of ion and electron number densities is not small. The large departure of electron number density from the Saha equilibrium value in each case implies insufficient recombination or ionization. The electron temperature elevation above the gas temperature is shown in Fig. 9 for Figs. 6-8. Even in the seeded combustion gas, the thermal nonequilibrium between electron and gas temperatures becomes large near the cold electrode surface with the increase of current density. This is because of the very high electric field in the low conductivity zone. In Fig. 10, the relation

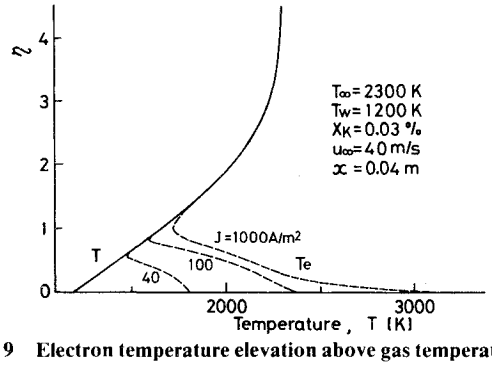

Fig. 9 Electron temperature elevation above gas temperature.

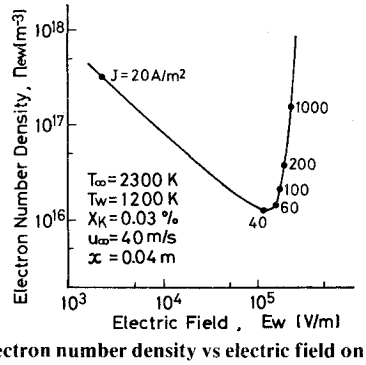

Fig. 10 Electron number density vs electric field on the surface.

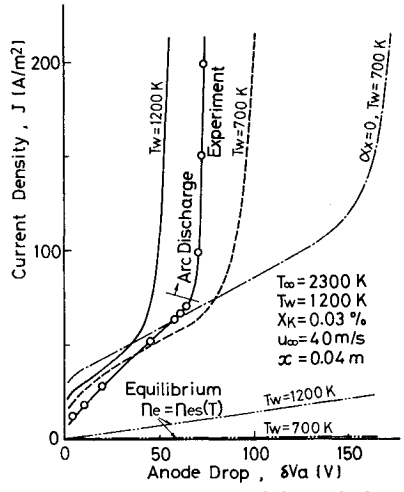

Fig. 11 Comparison of experimental and theoretical results—current density vs anode drop.

between the electron number density and the electric field at the electrode surface is shown for various current densities. For the low current density (the left branch in Fig. 10), the increase of current density is assured by the increase of the electric field in compensating the decrease of electron number density. For the high current density (the right branch in Fig. 10), the high electron number density and the charge separation secure the increase of current density, while the electric field is almost fixed at the order of 10^5 V/m.

B. Comparison of Experimental and Theoretical Results

The theoretical result of the anode voltage drop is compared with the experimental result in Fig. 11. This comparison is valid, in principle, in the diffusive mode discharge region. The double dot-dash lines show results calculated on the assumption that the electron number density is in Saha equilibrium at the local gas temperature $n_e = n_{es}(T)$ and proves that such a condition is not realized near the cold electrode. The fact that experimental results are distributed between two curves calculated for $T_w = 700$ K and $T_w = 1200$ K shows a partial existence of condensed seed material on the electrode. From the calculated curve for $\alpha_x = 0$, even though there still remains the uncertainty of the value of α_x, it is found that theoretical results are improved by the introduction of the three-body recombination process where the third body is a heavy particle in the analysis.

C. Turbulent Boundary-Layer Analysis

The aforementioned method used for the analysis of the laminar boundary layer is modified to be applied to the analysis of a turbulent boundary layer in a practical open-cycle MHD generator, which is featured by the large gas velocity, the long distance from the inlet, and the large current density. In spite of the very large current density in this case, only the case of diffusive current mode is considered in the study. The turbulent boundary-layer thickness is assumed to be given as $\delta = 0.371\, xRe_x^{-1/5}$, and the gas velocity profile is expressed by the one-seventh law. The turbulent Prandtl number and turbulent Schmidt number are assumed to be

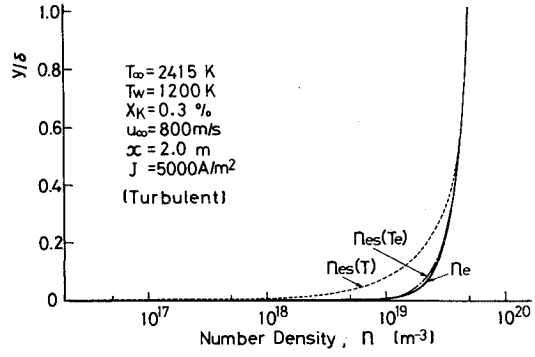

Fig. 12 Charged particle distribution in turbulent boundary layer.

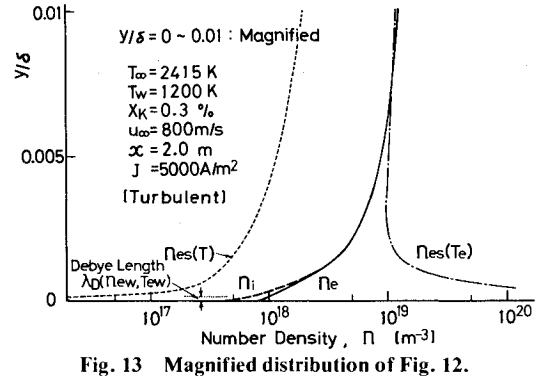

Fig. 13 Magnified distribution of Fig. 12.

unity, and the eddy viscosity is calculated from the mixing length, which is assumed to be constant over the outer region of the boundary layer and proportional to the distance from the surface in the inner region of it. Because of the very large current density, the effect of gas temperature elevation by Joule heating is taken into consideration and so the main flow temperature at the inlet 2300 K is elevated to 2415 K for $J=5000$ A/m^2 at the distance of 2 m from the inlet. Numerical results are shown in Figs. 12 and 13. (In Fig. 13, the ordinate is one hundred times larger than that in Fig. 12.) In spite of the large boundary-layer thickness and the low surface temperature, the charge separation region is limited to the extent of several Debye lengths, and this is because the effect of low surface temperature is not so significant in the turbulent boundary layer as in the laminar one. There exists little deviation of the electron number density from Saha equilibrium value for the local electron temperature except in the very thin layer near the surface. However, electron thermal nonequilibrium caused by the large current density is serious. It should be stressed that in this case corresponding to the practical MHD generator condition, the situation is very much different from that of the laminar case described earlier, and that the degrees of electron thermal and ionizational nonequilibria and the extent of the charge separation region depend much on the operating conditions such as Reynolds number, seed fraction, and current density.

V. Conclusions

The boundary layer of seeded combustion gas over a cold anode was numerically solved by use of a three-fluid model under the assumption of charge separation, electron thermal nonequilibrium, and ionizational nonequilibrium, and an experiment was conducted to make a comparison with the theory in connection with the voltage-current relation. The following conclusions have been obtained.

1) When the electrode temperature and the seed fraction are high, the conventional concepts of laminar combustion gas boundary layer, such as electron thermal and ionizational equilibria are realized, and electrical neutrality is proved to be correct.

2) When the electrode temperature is low, the electron number density becomes small near the electrode surface, electron-ion charge separation does occur to an extent much larger than the Debye length from the surface, and both electron thermal and ionizational nonequilibria become predominant even in the laminar seeded combustion gas.

3) As for the relation of the electron number density and the electric field on the surface, with an increase in the current density the electric field increases and the electron number density decreases in the small current density region, and the electron number density increases and the electric field is almost fixed at the order of 10^5 V/m in the large current density region.

4) It has been confirmed by the comparison of experimental and theoretical results in the laminar flow that, even in the seeded combustion gas, Saha equilibrium at the local gas temperature cannot be attained in the cold laminar boundary layer near the cold electrode surface.

5) In the turbulent boundary layer under the operating condition of an open-cycle MHD generator of practical scale, charge separation and ionizational nonequilibrium are not so remarkable as those in the laminar case, but for the large current density electron thermal nonequilibrium and gas temperature elevation by Joule heating are dominant, especially near the surface.

References

[1] Sherman, A., Yeh, H., Reshotko, E., and McAssey, E. Jr., "MHD Boundary Layers with Nonequilibrium Ionization and Finite Rates," AIAA Paper 71-139, New York, 1971.

[2] Brown, R. T., "Electron Temperature and Number Density Measurements in a Nonequilibrium Plasma Boundary Layer," Institute of Plasma Research, Stanford University, Stanford, Calif., SU-IPR Report No. 350, Jan. 1970.

[3] Cotte, D. W., "Ionizational and Electron Thermal Nonequilibrium in MHD Boundary Layers," *AIAA Journal*, Vol. 9, Dec. 1971, pp. 2404-2410.

[4] High, M. D. and Felderman, E. J., "Turbulent MHD Boundary Layers with Electron Thermal Nonequilibrium and Finite Rate Ionization," *AIAA Journal*, Vol. 10, Jan. 1972, pp. 98-103.

[5] Argyropoulos, G. S, Demetriades, S. T., Doss, E. D., and Oliver, D. A., "Electron Nonequilibrium in Open-Cycle MHD Generators," *AIAA Journal*, Vol. 12, May 1974, pp. 669-671.

[6] Maxwell, C. D., Demetriades, S. T., Argyropoulos, G. S., Patel, N. J., and Easterling, M., "Input Data for Computation of Thermodynamic and Electrical Properties of Coal Combustion Products," *13th Symposium on Engineering Aspects of Magnetohydrodynamics*, Paper VII. 5, 1973, Stanford, Calif.

[7] McDaniel, E. W. and Manson, E. A., *The Mobility and Diffusion of Ions in Gases*, Wiley, New York, 1973.

[8] Spencer, F. E. Jr. and Phelps, A. V., "Momentum Transfer Cross-Sections and Conductivity Integrals for Gases of MHD Interest," *15th Symposium on Engineering Aspects of Magnetohydrodynamics*, Paper IX. 9, 1976.

[9] Lam, S. H., "A General Theory for the Flow of Weakly Ionized Gases," *AIAA Journal*, Vol. 2, Feb. 1964, pp. 256-262.

[10] Hinnov, E. and Hirscheberg, J. C., "Electron-Ion Recombination in Dense Plasmas," *Physical Review*, Vol. 125, Feb. 1962, pp. 795-801.

[11] Mitchner, M. and Kruger, C. H., Jr., *Partially Ionized Gases*, Wiley, New York, 1973, pp. 266-272.